Double electron–electron resonance shows cytochrome P450cam undergoes a conformational change in solution upon binding substrate

Stefan Stoll[a,1,2], Young-Tae Lee[a,1], Mo Zhang[a], Richard F. Wilson[b], R. David Britt[a,3], and David B. Goodin[a,3]

[a]Department of Chemistry, University of California, One Shields Avenue, Davis, CA 95616; and [b]Department of Molecular Biology, The Scripps Research Institute, 10550 North Torrey Pines Road, La Jolla, CA 92037

Edited by Harry B. Gray, California Institute of Technology, Pasadena, CA, and approved June 25, 2012 (received for review April 27, 2012)

Although cytochrome P450cam from *Pseudomonas putida*, the archetype for all heme monooxygenases, has long been known to have a closed active site, recent reports show that the enzyme can also be crystallized in at least two clusters of open conformations. This suggests that the enzyme may undergo significant conformational changes during substrate binding and catalytic turnover. However, these conformations were observed in the crystalline state, and information is needed about the conformations that are populated in solution. In this study, double electron–electron resonance experiments were performed to observe substrate-induced changes in distance as measured by the dipolar coupling between spin labels introduced onto the surface of the enzyme on opposite sides of the substrate access channel. The double electron–electron resonance data show a decrease of 0.8 nm in the distance between spin labels placed at S48C and S190C upon binding the substrate camphor. A rotamer distribution model based on the crystal structures adequately describes the observed distance distributions. These results demonstrate conclusively that, in the physiologically relevant solution state, the substrate-free enzyme exists in the open P450cam-O conformation and that camphor binding results in conversion to the closed P450cam-C form. This approach should be useful for investigating many other P450s, including mammalian forms, in which the role of conformational change is of central importance but not well understood.

heme enzymes | distance measurement | electron paramagnetic resonance | spin-label | pulsed electron double resonance

Conformational change and flexibility play important roles in the function of many enzymes. The details of how an enzyme recognizes its substrate and activates its conversion to product are often discussed in terms of lock-and-key, induced fit, or conformational selection models (1–3). Such issues have been of central importance in understanding the substrate specificity of the large family of cytochromes P450 (4, 5). With nearly 12,000 members across all living organisms (6), these heme-containing monooxygenases use an external electron source to activate O_2 and insert oxygen into C-H bonds of a wide range of substrates (7). Although P450s exhibit a common protein fold and are believed to use a common reactive Compound I intermediate, they differ vastly in their substrate specificity. For example, many P450s involved in biosynthetic pathways carry out highly regio- and stereospecific reactions with substrate (8), while other forms, for example those involved in hepatic drug metabolism, can be very indiscriminate by allowing a single isozyme to oxidize a large variety of compounds (9). Much of this diversity is believed to arise from variations in the F and G helices, the intervening loop, and the adjacent B' helix, which fold around the substrate binding site at the distal heme face. Structurally distinct substrate binding sites have been observed for bacterial (4, 10, 11), microsomal (12–15), and mitochondrial P450s (16). In addition, several P450s have been observed to undergo significant conformational change in these structural elements upon substrate or inhibitor binding (17–22). However, it remains unclear whether conformational change plays an important role in all P450s. Thus, the extent to which substrate recognition is coupled to conformational gating of important functional events including electron transfer and O-O bond cleavage has remained incompletely understood.

Our understanding of the effects of substrate on the conformation of P450cam (CYP101A1), the camphor metabolizing P450 from *Pseudomonas putida*, has changed over time. Important early studies have suggested that it has an active site that is relatively static in response to substrate binding (4, 10, 23). Based on the comparison of X-ray structures obtained for the enzyme when it is crystallized in the presence of camphor and when small ligands such as dithiothreitol (DTT) are soaked out of the crystals, it was suggested that the enzyme undergoes only minor conformational changes upon binding substrate (10, 23). However, the question of how camphor enters the buried, solvent-inaccessible binding site of the closed form remained unresolved (4). Crystal structures of an open conformation, observed in the presence of large tethered substrate analogs, provided a proposal for the substrate access route (24, 25) through a substrate channel, but it remained initially uncertain how much these tethered substrate analogs were perturbing the native conformation. Thus, it was significant when P450cam was reported to visit the same open conformation when crystallized in the absence of any substrate (26). This suggested that crystal packing interactions may have prevented substrate-dependent conformational changes in the experiments where DTT was soaked out of crystals (23). A recent study of the structures of P450cam bound to a family of tethered substrates showed that the enzyme can be observed in at least three distinct clusters of conformations, representing open (P450cam-O), intermediate (P450cam-I), and closed (P450cam-C) states (27) that result primarily from segmental movements of the F and G helices. These observations have provided support for the proposal that in solution, P450cam undergoes significant conformational changes in the F and G helices during substrate binding and turnover. However, these conformations were observed for the protein in the crystalline state, and information is currently lacking about the conformations that are actually populated in the physiologically relevant solution state. This issue is

Author contributions: D.B.G., R.D.B., Y.-T.L., and S.S. designed the research; S.S., Y.-T.L., and M.Z. performed the research; Y.-T.L. and R.F.W. provided new materials and sample characterization; S.S. analyzed the data; and S.S., Y.-T.L., D.B.G. and R.D.B. wrote the paper.

The authors declare no conflict of interest.

This article is a PNAS Direct Submission.

Freely available online through the PNAS open access option.

Data deposition: The atomic coordinates and structure factors have been deposited in the Protein Data Bank, www.pdb.org (PDB ID code 4EK1).

[1]S.S. and Y.-T.L. contributed equally to this work.

[2]Present address: Department of Chemistry, University of Washington, Seattle, WA 98195.

[3]To whom correspondence may be addressed. E-mail: dbgoodin@ucdavis.edu or rdbritt@ucdavis.edu.

This article contains supporting information online at www.pnas.org/lookup/suppl/doi:10.1073/pnas.1207123109/-/DCSupplemental.

particularly important given the recent report of NMR studies (28), which demonstrate significant changes in the conformational ensemble upon camphor binding, but did not reveal large movements in the F and G helices. Therefore, it has become critically important to establish whether the previously reported open conformations are seen in the solution state.

In this report, double electron–electron resonance (DEER) spectroscopy of spin-labeled P450cam is used to clarify these issues by providing conformational information for P450cam in solution, specifically determining the position of the F-G loop relative to the rest of the enzyme in the presence and absence of camphor. This study also demonstrates how this method may prove generally useful for probing conformational changes in many other forms of P450 for which such information is both desirable and difficult to obtain.

Results

Two spin labels were introduced onto the surface of P450cam to allow observation of the change from the open to closed conformation in solution by measurement of the inter-spin through-space magnetic dipolar coupling. To facilitate the use of thiol-specific spin labels, surface accessible wild-type cysteines were first mutated to serine. Wild-type P450cam contains eight cysteine residues. C334, the most reactive surface cysteine, is routinely changed to alanine for studies by our laboratory and many others to prevent intermolecular disulfide formation (29). Four cysteines (C58, C85, C136, and C285) that are at least partially exposed on the surface of the enzyme were also replaced with serine to give P450cam-(4S) containing no surface accessible thiols. The remaining three cysteines are not reactive: C148 and C242 are partially buried, and C357 is coordinated to the heme. A comparison of the crystal structures for camphor-bound P450cam-C and camphor-free P450cam-O (Fig. 1) shows that the distance between the F-G loop and the residues across the substrate channel (around helix A and strand β1) is maximally sensitive to changes in the open-to-closed transition. S48 and S190 are surface-exposed serines with their side chains directed toward solvent and were thus considered good candidates for mutation to cysteine and spin label attachment. S48, near the A helix, does not change position relative to the core of the protein during the conformational change, while residue S190, in the middle of the F-G loop, moves toward S48 by 0.8 nm upon closure of the substrate channel (Fig. 1). Thus, the S48C and S190C mutations were introduced into the P450cam-(4S) background to generate P450cam-(4S,2C). Samples of purified P450cam-(4S) and P450cam-(4S,2C) protein displayed 0.01 and 1.82 reactive thiols, respectively, as shown by the Ellman reaction (30). UV-visible spectra showed that the ferric heme in P450cam-(4S, 2C) is converted from a low-spin state ($\lambda_{max} = 417$ nm) in the absence of camphor to a predominantly high-spin state ($\lambda_{max} = 392$ nm) upon addition of 1 mM camphor (Fig. S1), consistent with the characteristic behavior of wild-type P450cam. Following spin labeling of P450cam-(4S,2C) with the perdeuterated spin label MTSL-d_{15} (d_{15}-2, 5-dihydro-2, 2, 5, 5-tetramethyl-3-[[(methylsulfonyl)thio]methyl]-1H-pyrrol-1-yloxy) and removal of unreacted spin label by gel filtration, approximately 1.6 spin labels per protein were observed by double integration of CW EPR spectra (Fig. S2) and comparison to a CuEDTA standard. Finally, the crystal structure at 2.0-Å resolution was determined for spin-labeled P450cam-(4S,2C) in the camphor-bound closed form (Table S1). The electron density for one of two molecules in the asymmetric unit clearly indicated the presence of the spin labels extending from the S48C and S190C sulfur atoms. This density fit well to a single conformation of MTSL built into the model, from which the inter-spin distance in the closed form was measured at 4.4 nm (Fig. 2). Electron density for the spin labels in the second molecule of the asymmetric unit were not as clearly defined suggesting some conformational disorder.

DEER experiments were performed to measure substrate-induced changes in magnetic dipolar coupling between the two spin labels on P450cam. Fig. 3*A* shows the experimental DEER time traces. The frequencies of the oscillations are determined by the magnetic dipolar coupling between the unpaired electrons of the two spin labels which, in turn, is proportional to the inverse cube of the distance r_{NO} between the centers of the spin label N-O bonds, $\nu_{dip} = (52\ \text{MHz})(r_{NO}/\text{nm})^{-3}$. The higher frequency for the substrate-bound form clearly demonstrates a reduced distance between the two spin labels compared to the substrate-free form. In both cases, the significant damping of the echo modulation amplitude over time indicates that there is a heterogeneous distribution of distances rather than a single distance. The corresponding distance distributions, extracted from the time traces using Tikhonov regularization (31), are shown in Fig. 3*B* and are dominated by peaks at 5.6 nm and 4.8 nm, respectively, for samples in the absence and presence of camphor. The distance distributions therefore show a 0.8-nm reduction in distance upon substrate binding. This is in agreement with the difference predicted from the crystal structures for conversion from the P450cam-O to the P450cam-C conformation (Fig. 1). Smaller peaks in the distance distribution at approximately 3 nm in Fig. 3*B* may result from artifacts due to deuterium modulation of the spin labels, or from effects of the coupling between the spin labels and the Fe(III) center. The small peak at approximately 8 nm for the substrate-free form is assigned to incomplete removal of inter-molecular modulation background. For the closed conformation, the distance of 4.8 nm observed experimentally by DEER (Fig. 3*B*) is in reasonable agreement with the value of 4.4 nm observed in the crystal structure of the labeled protein (Fig. 2).

Modeling of the spin label side-chain conformations and their disorder on the surface of the enzyme largely accounts for the distance distribution width, providing additional insight. Starting from the crystal structures of open and closed states, the r_{NO} distributions were estimated computationally using a conforma-

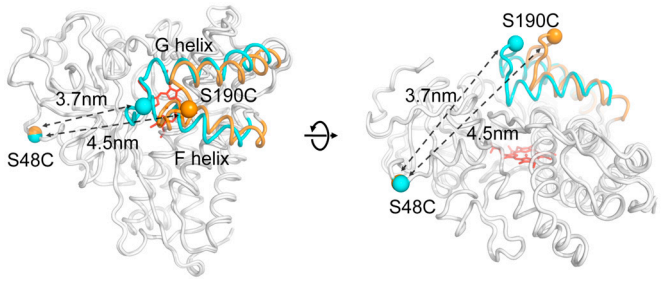

Fig. 1. Crystal structures of P450cam in the closed substrate-bound (cyan, pdb 2CPP) and open substrate-free (orange, PDB ID code 3L61) conformations. For clarity, only the most displaced regions, including the helices F and G and the connecting loop, are colored. Cα positions are labeled at the S48C and S190C mutation sites. Heme is shown in red.

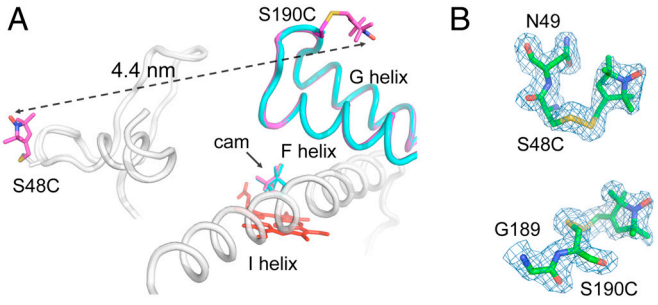

Fig. 2. Crystal structure of spin-labeled P450cam-(4S,2C) in the closed substrate-bound conformation. (*A*) Spin labeled mutant (magenta, PDB ID code 4EK1) and wild type (cyan, PDB ID code 2CPP) are superimposed. For clarity, only secondary structures around the spin labeling sites and the I helix are shown. (*B*) 2Fo-Fc map of the labeling sites, contoured at 1σ.

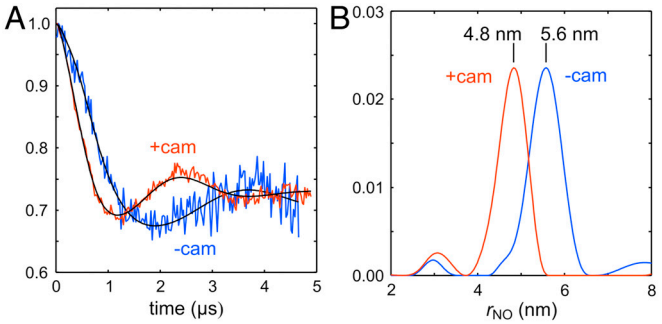

Fig. 3. (*A*) Experimental (color) and fitted (black) DEER time traces for substrate-free (−cam, blue) and camphor-bound (+cam, red) cytochrome P450cam-(4S,2C) spin labeled at positions S48C and S190C. (*B*) DEER distance distributions as a function of the distance between the NO groups of the two spin labels (r_{NO}), obtained from Tikhonov regularization of the experimental DEER traces.

tional distribution model based on a rotameric library for MTSL (32) and the crystal structures of the unlabeled enzyme, which were kept rigid. Fig. 4*A* illustrates the predicted disorder of the NO spatial location at the S48C and S190C labeling sites, resulting in the distance distributions shown by dotted lines in Fig. 4*B* and summarized in Tables S2–S4. The modeled distributions of Fig. 4*B* remain 0.3–0.4 nm shorter than the experimentally determined DEER distance distributions. In the camphor free state, the width of the observed distribution is very similar to that modeled by conformational flexibility of the 5 dihedral angles within MTSL (32). In the camphor bound state, the observed distribution is a little narrower than that modeled. Although these effects might be sensitive to the glass-transition temperature of the solvation shell around the protein, assumed to be 175 K in the calculations (33), or to partial orientation selection in the experiment (34), these results suggest that the distribution

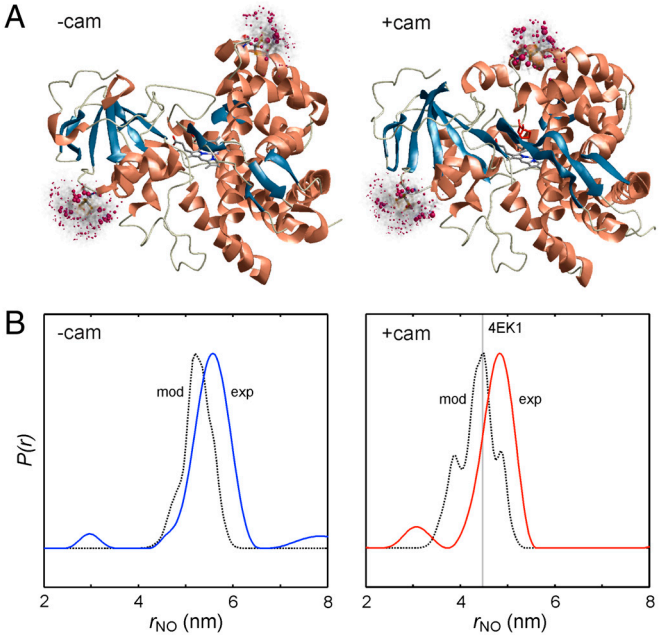

Fig. 4. (*A*) Rotameric models of substrate-free (−cam, PDB ID code 3L61) and substrate-bound (+cam, PDB ID code 2CPP) forms of cytochrome P450cam spin-labeled with MTSL at positions S48C and S190C. The spheres indicate the positions of the NO group in the various rotamers, and sphere diameters are proportional to the fractional populations. (*B*) Comparison of modeled (dashed) and experimental (solid) distance distributions for substrate-bound and substrate-free P450cam. The gray line represents the observed distance between NO bond centers in the crystal structure of spin-labeled P450cam +cam (PDB 4EK1; see Fig. 2).

widths of r_{NO} observed in the DEER experiments are dominated by torsional disorder of the spin label rather than by the protein backbone Cα–Cα distance distribution.

Discussion

Role of Conformational Change. Despite much effort over many decades, the molecular basis of substrate specificity in P450s is not fully understood, and recent results suggest a shifting paradigm that may have broad impact on our understanding of their function. Even P450cam, the most well studied example, has recently been trapped in multiple conformations in response to binding of tethered substrate analogues (27). These results suggest P450cam might be similar to other P450 enzymes, which have been observed to undergo significant conformational changes in response to substrate or ligand binding (35–38). Still, it remains possible that the substrate channel of some P450s is more flexible than others and thus, the role played by conformational change and dynamics in defining substrate specificity of a particular form remains unresolved. The current study clarifies these issues for the solution state of P450cam and suggests that DEER spectroscopy may be used with this and other forms of P450 to gain a greater insight into these questions.

Crystal vs. Solution. The recent observation of multiple conformations of P450cam in response to binding a library of tethered substrates (27) demonstrates the range of structures that can be sampled by a given form of the enzyme and suggests how substrates enter and leave the binding site of the closed conformation. However, these states have been characterized in the crystalline state, and additional information about which conformations are populated in solution is needed. The different structures obtained for the substrate-free enzyme depending on whether the substrate is soaked out of crystals (23) or is absent during crystallization (26) suggest that crystal contacts might influence the conformational equilibrium and warn that the states seen in the crystal do not necessarily reflect those populated in solution. In addition, while a recently reported NMR study (28) has shown that camphor binding results in alteration of the conformational ensemble in solution, large-scale movements of the F and G helices were not indicated. It was suggested that crystal contacts may be responsible for this difference, but it is possible that the presence of CO in the NMR studies may also contribute to changing the conformational equilibrium. A complete picture will likely require a combination of techniques. Thus, the use of DEER spectroscopy to quantitatively observe conformational changes in solution provides crucial new information about the basic function of this model enzyme.

Distances and Their Changes. For the camphor bound closed conformation, the absolute distance between spin labels determined by DEER is in good agreement with the crystal structure of the spin-labeled protein. In general, the inter-spin distances are about 0.5–0.7 nm longer than the backbone distances between the residues (see Table S3) due to the tether of the two spin label side chains. By themselves, the absolute distance values are therefore difficult to interpret. On the other hand, the clear change in spin label distance observed by DEER in response to substrate binding is direct evidence for substrate-induced closure of the substrate channel. The similarity of the substrate-induced −0.8 nm distance change observed by DEER and that predicted from X-ray crystallography strongly supports the conclusion that the substrate-free enzyme exists in the open P450cam-O conformation and that camphor binding results in conversion to the closed P450cam-C form. Thus, in the present case, the conformational states characterized by X-ray crystallography appear to accurately reflect the forms populated in solution, provided that the crystals are grown in equilibrium with the final substrate concentration. The DEER data show that the substrate-free and

substrate-bound forms in solution are predominantly in the open and closed conformations, respectively (Fig. 3*B*). In addition, the DEER data provide no evidence for a significant population of the P450cam-I intermediate conformation observed in the presence of some tethered substrates (27).

Distance Distributions. An important feature of DEER spectroscopy is its ability to provide information about the distribution of distances in the sample. A heterogeneity in the distance results in the damping of the echo modulation amplitude, which can be characterized if the acquired data extends long enough in time. In the present case, careful optimization of experimental conditions, high purity of the samples and the use of deuterated buffer components and spin labels (see *Methods*) allowed DEER data collection up to 5 μs, enough to observe significantly more than one full cycle of echo modulation for both samples. As a result, distance distributions were obtained in which not only the distribution modes but also the distribution widths are significant. However, the DEER traces are too short to allow interpretation of the shape of the distance distributions. Further studies on deuterated protein (39) may allow refinement of DEER measurements such that better resolved distribution shapes are obtained and substrate binding events can be probed beyond the simple two-state conformational model used here. This could possibly yield evidence for the multi-step conformational pathway that has recently been proposed for this enzyme (27).

Rotamer Analysis. As shown in Fig. 4*B* and in *SI Text*, the rotameric modeling based on the crystal structures yielded distance distributions that are in reasonable agreement with experiment. The distances predicted based on the crystal structures of the unlabeled enzyme are slightly shorter than those experimentally observed by DEER in the solution state. Remarkably, when the crystal structure of the spin-labeled enzyme was used for distance distribution modeling, the predicted and experimental distances distribution modes coincide (Fig. S3), suggesting that small changes in the local structure around the labeling sites can affect the accuracy of rotamer modeling. The systematic deviation of the predicted distance distributions from the experimental DEER results might be a result of the approximate nature of the rotamer library approach, which is known to yield biased results in some cases (32, 40). Also, it is possible that the use of the crystal structures in place of the unknown solution structures contributes to the discrepancy because the regions around one or both labeling sites might have solution conformations that are different from those in the crystal structure (Figs. S4 and S5). On the other hand, the spin label side chain might interact with specific residues on the protein surface in a way not captured by the rotamer model (e.g., via hydrogen bonds), and thus only a subset of the modeled rotameric states shown in Fig. 4 might be populated. In the case of a specific label-protein interaction, some of the width of the observed distance distributions could then arise from heterogeneity of protein backbone conformation. This possibility is under investigation and can be tested by additional DEER studies on mutants near the labeling sites.

Mechanism. Based on our results it seems very likely that substrate binding in P450cam is facilitated by the conformational flexibility of the enzyme. In the absence of substrate, the open form P450cam-O appears to be energetically most favored. Based on present data, it is not clear whether this is the only conformation that is (statically) populated at physiological temperature or whether there is dynamic exchange within an ensemble of thermally accessible conformations. The latter would be consistent with the DEER data only if the conformations do not differ significantly in their 48–190 distances. Upon passage of the substrate through the channel into the active site, the energetics of the conformational landscape is changed such that the closed form P450cam-C is most stable. This open-closed transition can either be a substrate-directed induced-fit process or a dynamic relaxation of the enzyme into the new conformational energetic landscape. Structural studies using tethered substrate analogues (27) suggest a prominent intermediate conformation state along the open-closed transition, with a possible role of putidaredoxin as conformational or functional effector (41–43). Conformational changes associated with substrate recognition, enzyme reduction and O_2 binding may be coupled to the position of the catalytically important water and Thr-252 side chain (44). It has been shown that the product complex closely resembles the closed substrate-bound conformation (45), and thus product release would necessitate reopening of the substrate channel. The release mechanism and its trigger are currently not fully understood.

In conclusion, the DEER-based coarse-grain structural analysis approach used in this work provides new insight into the mechanism of substrate binding in P450cam. It should be useful for investigating conformational states of many other P450s, for example mammalian forms, that are proposed to undergo conformational changes during substrate recognition, but for which key structural information is lacking.

Methods

Mutant Construction and Protein Purification. Mutations were introduced into the plasmid DNA (pETCAM-C334A) for *Escherichia coli* expression of P450cam using methods previously described and verified by DNA sequencing. In preparation for site-specific spin-labeling of P450cam, reactive surface exposed cysteines were first removed by mutation to serine. These sites included C58S, C85S, C136S, and C285S in addition to the C334A mutation normally used by our laboratory to prevent protein dimerization. The resulting construct, labeled P450cam-(4S), was used as a background to introduce a pair of surface cysteines at residues S48 and S190 to generate the construct denoted P450cam-(4S, 2C) for spin label attachment.

Protein expression and purification utilized methods previously described for P450cam-C334A (26). One mM dithiothreitol (DTT) was included in all buffers to prevent intermolecular disulfide bond formation. Protein stock solutions were stored at −80 °C in 50 mM potassium phosphate (pH 6.0), 300 mM KCl, 1 mM camphor and 1 mM DTT. The Ellman reaction was used to determine the number of reactive surface thiols on the protein. Briefly, protein was incubated (5 min at RT) in 100 μM DTNB (5,5′-dithio-bis(2-nitrobenzoic acid)), 1 mM camphor and 100 mM Tris (pH 8.0). The optical absorbance at 412 nm ($\varepsilon_{412} = 13{,}600\ M^{-1}\,cm^{-1}$) was used for calculation of concentration of free thiol concentration and was corrected for the contribution of heme to the absorbance using control samples omitting DNTB.

Spin Labeling and EPR Sample Preparation. P450cam-(4S, 2C) was labeled with either MTSL (2,5-dihydro-2,2,5,5-tetramethyl-3-[[(methylsulfonyl)thio] methyl]-1H-pyrrol-1-yloxy, (1-oxyl-2,2,5,5-tetramethyl-Δ3-pyrroline-3-methyl) methanethiosulfonate) (Toronto Research Chemicals) or its perdeuterated derivative, MTSL-d_{15}. DTT was first removed from the protein by buffer exchange into 50 mM Tris (pH 7.4) by gel filtration using two sequential PD-10 columns (GE Healthcare). Camphor (1 mM) and KCl (200 mM) were added before incubating for 10 min at 4 °C in a 10-fold molar excess of the spin label. The reaction was quenched by removal of excess of MTSL by gel filtration through a PD-10 column. EPR samples of spin-labeled ferric P450cam were prepared at a final protein concentration of ca. 150 μM by exchange into buffer made from 99% D_2O containing 50 mM Tris (pD 7.8), 200 mM KCl, 1 mM camphor (omitted in the substrate-free sample) and 30% d_8-glycerol (Cambridge Isotopes Laboratory). For each sample, 150 μL was loaded into a 4 mm o.d. quartz tube (Wilmad 706-PQ-9.50) and flash frozen in liquid nitrogen.

Crystallization, Data Collection, and Structure Determination. Crystals of spin-labeled P450cam-(4S,2C) were grown from 50 mM Tris, pH 7.4, 200 mM KCl, 1 mM camphor and 12% PEG 8000. Crystals were transferred to the mother liquor with additional 25% PEG 600 and flash frozen on nylon loops. X-ray diffraction data were collected at 100 K on the beamline 7-1 at the Stanford Synchrotron Radiation Laboratory. Data processing, molecular replacement, refinement, and validation were carried out with the same methods employed previously (26). Statistics for data collection and refinement are shown in Table S1. The atomic coordinates and structure factors have been deposited in the Protein Data Bank (PDB ID code 4EK1). Two protein molecules are present in the asymmetric unit. MTSL was modeled into observed

electron density maps at S48C and S190C in molecule A and at S48C in molecule B but not at S190C of molecule B due to disorder. Structural illustrations were generated using the Pymol Molecular Graphics System (46).

EPR Data Collection and Analysis. X-band continuous-wave (CW) EPR spectra were measured at the CalEPR Center at UC Davis on a Bruker ECS106 spectrometer at 9.5 GHz/0.34 T using a Bruker SHQE resonator and an Oxford liquid helium cooling system. The EPR signals of low- and high-spin ferric iron from the heme (47) did not interfere with the nitroxide measurements because the Fe^{3+} signals in the nitroxide region are very weak due to their large anisotropy compared to the nitroxide signal. The concentration of spin labels was determined by comparison of the double integral of the spin label spectrum to the double integral of a CuEDTA solution with known concentration.

X-band DEER data were acquired at the CalEPR Center at UC Davis on a Bruker EleXsys E580 spectrometer at 9.5 GHz using a Bruker MD4 dielectric resonator and an Oxford liquid helium cooling system, at temperatures between 20 and 50 K and a magnetic field of about 340 mT. The DEER pulse sequence $(\pi/2)_1 - \tau_1 - (\pi)_1 - \tau_1 + t - (\pi)_2 - (\tau_2 - t) - (\pi)_1 - \tau_2 - [\text{echo}]$ was used with pulse lengths of 16/32/32 ns for the probe pulses (subscript 1) and 32 ns for the pump pulse (subscript 2). The value of τ_1 was adjusted to a maximum in the ^{2}H nuclear modulation envelope (400 ns), and t was varied between −40 ns and about 5 μs in increments of 12 or 20 ns. Averaging over τ_1, which could cancel potential distance artifacts due to deuterium or proton modulations (48), could not be performed due to an insufficient signal-to-noise ratio. The pump frequency ν_2 was centered in the resonator mode and aligned with the spectral maximum. The probe frequency ν_1 was 65 MHz above ν_2.

Deuteration of the buffer was crucial for the DEER measurements because it prolonged the phase memory time, T_M, allowing data acquisition in which t extended to 5 μs (total pulse sequence length almost 11 μs). Additional per-deuteration of the spin label gave an additional 10% increase in T_M, but also introduced deep modulations as a function of τ_1.

For the substrate-bound form, the best data were obtained at 50 K. At lower temperatures, the modulations were shallower and the damping was stronger, probably due to saturation effects. For the substrate-free form, relaxation at 50 K was too fast to allow the acquisition of an entire 5 μs long time trace, so data were acquired at 30 K where relaxation is slower.

EPR spectral simulations and quantitations were performed using EasySpin 4.0 (49). The DEER data were analyzed and fit with DeerAnalysis2011 (31). Rotameric modeling was performed with MMM2011 (32).

ACKNOWLEDGMENTS. The authors acknowledge the assistance of J. Rosenberg and helpful discussions with Professors T.L. Poulos, J.R. Halpert, E.F. Johnson, C.D. Stout, and J.B. Ames. This work was supported by the National Institutes of Health (GM41049 to D.B.G.) and the Department of Energy (DE-FG02-09ER16117 to R.D.B.). Portions of this research were carried out at the Stanford Synchrotron Radiation Lightsource, a Directorate of SLAC National Accelerator Laboratory and an Office of Science User Facility operated for the U.S. Department of Energy Office of Science by Stanford University. The SSRL Structural Molecular Biology Program is supported by the DOE Office of Biological and Environmental Research, and by the National Institutes of Health, National Institute of General Medical Sciences (including P41GM103393) and the National Center for Research Resources (P41RR001209). The contents of this publication are solely the responsibility of the authors and do not necessarily represent the official views of NIGMS, NCRR or NIH.

1. Koshland DE (1958) Application of a theory of enzyme specificity to protein synthesis. *Proc Natl Acad Sci USA* 44:98–104.
2. Boehr DD, Nussinov R, Wright PE (2009) The role of dynamic conformational ensembles in biomolecular recognition. *Nat Chem Biol* 5:789–796.
3. Henzler-Wildman K, Kern D (2007) Dynamic personalities of proteins. *Nature* 450:964–972.
4. Pylypenko O, Schlichting I (2004) Structural aspects of ligand binding to and electron transfer in bacterial and fungal P450s. *Annu Rev Biochem* 73:991–1018.
5. Poulos TL, Johnson EF (2005) Structures of cytochrome P450 enzymes. *Cytochrome P-450: Structure, Mechanism, and Biochemistry,* ed PR Ortiz de Montellano (Kluwer Academics/Plenum, New York), 3rd Ed,, pp 87–114.
6. Nelson DR (2009) The cytochrome p450 homepage. *Hum Genomics* 4:59–65.
7. Ortiz de Montellano PR (2009) Hydrocarbon hydroxylation by cytochrome P450 enzymes. *Chem Rev* 110:932–948.
8. Pikuleva IA (2006) Cytochrome P450s and cholesterol homeostasis. *Pharmacol Ther* 112:761–773.
9. Wienkers LC, Heath TG (2005) Predicting in vivo drug interactions from in vitro drug discovery data. *Nat Rev Drug Discov* 4:825–833.
10. Poulos TL, Finzel BC, Howard AJ (1987) High-resolution crystal structure of cytochrome P450cam. *J Mol Biol* 195:687–700.
11. Cupp-Vickery JR, Poulos TL (1995) Structure of cytochrome P450eryF involved in erythromycin biosynthesis. *Nat Struct Biol* 2:144–153.
12. Scott EE, et al. (2003) An open conformation of mammalian cytochrome P450 2B4 at 1.6-Å resolution. *Proc Natl Acad Sci USA* 100:13196–13201.
13. Scott EE, et al. (2004) Structure of mammalian cytochrome P450 2B4 complexed with 4-(4-chlorophenyl)imidazole at 1.9-Å resolution: Insight into the range of P450 conformations and the coordination of redox partner binding. *J Biol Chem* 279:27294–27301.
14. Williams PA, et al. (2003) Crystal structure of human cytochrome P450 2C9 with bound warfarin. *Nature* 424:464–468.
15. Johnson EF, Stout CD (2005) Structural diversity of human xenobiotic-metabolizing cytochrome P450 monooxygenases. *Biochem Biophys Res Commun* 338:331–336.
16. Annalora AJ, et al. (2010) The crystal structure of CYP24A1, a mitochondrial cytochrome P450 involved in vitamin D metabolism. *J Mol Biol* 396:441–451.
17. Li H, Poulos TL (1997) The structure of the cytochrome p450BM-3 haem domain complexed with the fatty acid substrate, palmitoleic acid. *Nat Struct Biol* 4:140–146.
18. Ouellet H, Podust LM, Ortiz de Montellano PR (2008) Mycobacterium tuberculosis CYP130: Crystal structure, biophysical characterization, and interactions with antifungal azole drugs. *J Biol Chem* 283:5069–5080.
19. Park SY, et al. (2002) Thermophilic cytochrome P450 (CYP119) from *Sulfolobus solfataricus*: High resolution structure and functional properties. *J Inorg Biochem* 91:491–501.
20. Xu LH, Fushinobu S, Ikeda H, Wakagi T, Shoun H (2009) Crystal structures of cytochrome P450 105P1 from *Streptomyces avermitilis*: Conformational flexibility and histidine ligation state. *J Bacteriol* 191:1211–1219.
21. Yano JK, et al. (2000) Crystal structure of a thermophilic cytochrome P450 from the archaeon Sulfolobus solfataricus. *J Biol Chem* 275:31086–31092.
22. Zhao B, Guengerich FP, Voehler M, Waterman MR (2005) Role of active site water molecules and substrate hydroxyl groups in oxygen activation by cytochrome P450 158A2: A new mechanism of proton transfer. *J Biol Chem* 280:42188–42197.
23. Poulos TL, Finzel BC, Howard AJ (1986) Crystal structure of substrate-free *Pseudomonas putida* cytochrome P-450. *Biochemistry* 25:5314–5322.
24. Dunn AR, et al. (2002) Fluorescent probes for cytochrome P450 structural characterization and inhibitor screening. *J Am Chem Soc* 124:10254–10255.
25. Hays AMA, et al. (2004) Conformational states of cytochrome P450cam revealed by trapping of synthetic molecular wires. *J Mol Biol* 344:455–469.
26. Lee Y-T, Wilson RF, Rupniewski I, Goodin DB (2010) P450cam visits an open conformation in the absence of substrate. *Biochemistry* 49:3412–3419.
27. Lee Y-T, Glazer EC, Wilson RF, Stout CD, Goodin DB (2011) Three clusters of conformational states in P450cam reveal a multistep pathway for closing of the substrate access channel. *Biochemistry* 50:693–703.
28. Asciutto EK, Young MJ, Madura J, Pochapsky SS, Pochapsky TC (2012) Solution structural ensembles of substrate-free cytochrome P450(cam). *Biochemistry* 51:3383–3393.
29. Nickerson DP, Wong LL (1997) The dimerization of Pseudomonas putida cytochrome P450cam: Practical consequences and engineering of a monomeric enzyme. *Protein Eng* 10:1357–1361.
30. Ellman GL (1959) Tissue sulfhydryl groups. *Arch Biochem Biophys* 82:70–77.
31. Jeschke G, et al. (2006) DeerAnalysis2006—a comprehensive software package for analyzing pulsed ELDOR data. *Appl Magn Reson* 30:473–498.
32. Polyhach Y, Bordignon E, Jeschke G (2011) Rotamer libraries of spin labelled cysteines for protein studies. *Phys Chem Chem Phys* 13:2356–2366.
33. Doster W (2010) The protein-solvent glass transition. *Biochim Biophys Acta* 1804:3–14.
34. Lovett JE, et al. (2009) Structural information from orientationally selective DEER spectroscopy. *Phys Chem Chem Phys* 11:6840–6848.
35. Savino C, et al. (2009) Investigating the structural plasticity of a cytochrome P450: Three dimensional structures of P450 EryK and binding to its physiological substrate. *J Biol Chem* 284:29170–29179.
36. Sherman DH, et al. (2006) The structural basis for substrate anchoring, active site selectivity, and product formation by P450 PikC from *Streptomyces venezuelae*. *J Biol Chem* 281:26289–26297.
37. Muralidhara BK, Sun L, Negi S, Halpert JR (2008) Thermodynamic fidelity of the mammalian cytochrome P450 2B4 active site in binding substrates and inhibitors. *J Mol Biol* 377:232–245.
38. Gay SC, Sun L, Maekawa K, Halpert JR, Stout CD (2009) Crystal structures of cytochrome P450 2B4 in complex with the inhibitor 1-biphenyl-4-methyl-1H-imidazole: Ligand-induced structural response through alpha-helical repositioning. *Biochemistry* 48:4762–4771.
39. Ward R, et al. (2010) EPR distance measurements in deuterated proteins. *J Magn Reson* 207:164–167.
40. Lillington JED, et al. (2011) Shigella flexneri Spa15 crystal structure verified in solution by double electron electron resonance. *J Mol Biol* 405:427–435.
41. Pochapsky SS, Pochapsky TC, Wei JW (2003) A model for effector activity in a highly specific biological electron transfer complex: The cytochrome P450(cam)-putidaredoxin couple. *Biochemistry* 42:5649–5656.
42. Nagano S, Tosha T, Ishimori K, Morishima I, Poulos TL (2004) Crystal structure of the cytochrome P450cam mutant that exhibits the same spectral perturbations induced by putidaredoxin binding. *J Biol Chem* 279:42844–42849.
43. Tosha T, et al. (2003) NMR study on the structural changes of cytochrome P450cam upon the complex formation with putidaredoxin. Functional significance of the putidaredoxin-induced structural changes. *J Biol Chem* 278:39809–39821.

44. Schlichting I, et al. (2000) The catalytic pathway of cytochrome P450cam at atomic resolution. *Science* 287:1615–1622.
45. Li HY, Narasimhulu S, Havran LM, Winkler JD, Poulos TL (1995) Crystal structure of cytochrome P450cam complexed with its catalytic product, 5-exo-hydroxycamphor. *J Am Chem Soc* 117:6297–6299.
46. DeLano WL (2002) The PyMOL Molecular Graphics System. (DeLano Scientific LLC, San Carlos, CA).
47. Lipscomb JD (1980) Electron paramagnetic resonance detectable states of cytochrome P-450cam. *Biochemistry* 19:3590–3599.
48. Jeschke G (2012) DEER distance measurements on proteins. *Annu Rev Phys Chem* 63:419–446.
49. Stoll S, Schweiger A (2006) EasySpin, a comprehensive software package for spectral simulation and analysis in EPR. *J Magn Reson* 178:42–55.

Supporting Information

Stoll et al. 10.1073/pnas.1207123109

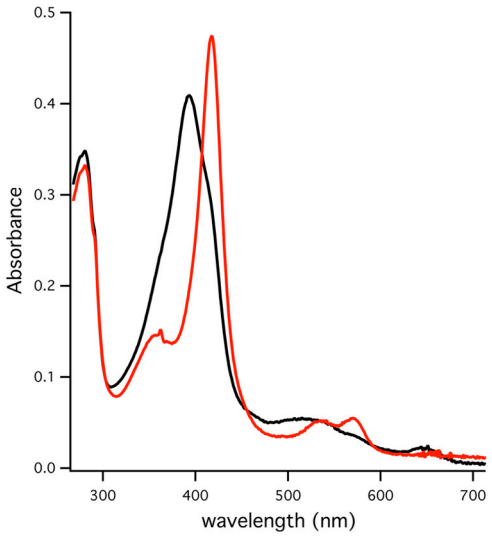

Fig. S1. UV/vis changes for P450cam-(4S,2C) on binding camphor. UV-vis spectra of DEER samples were measured just before freezing samples for DEER experiments. Spectra of substrate-free and camphor-bound samples are shown in red and black, respectively.

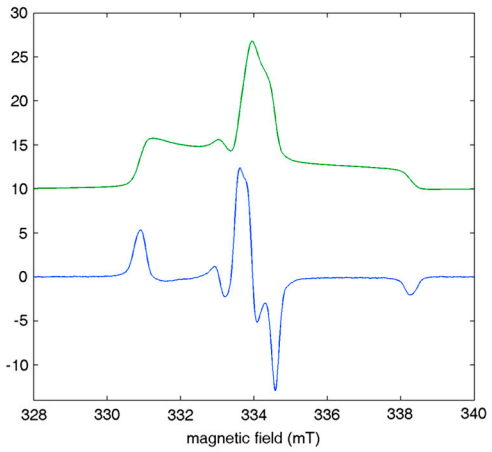

Fig. S2. CW EPR spectrum of protein P450cam-(4S,2C) spin labeled with d_{15}-MTSL in D_2O/d_8-glycerol, obtained at 100 K, 9.384 GHz and 1 μW. *Bottom* (blue): acquired spectrum with 0.1 mT field modulation amplitude. *Top* (green): integral of spectrum.

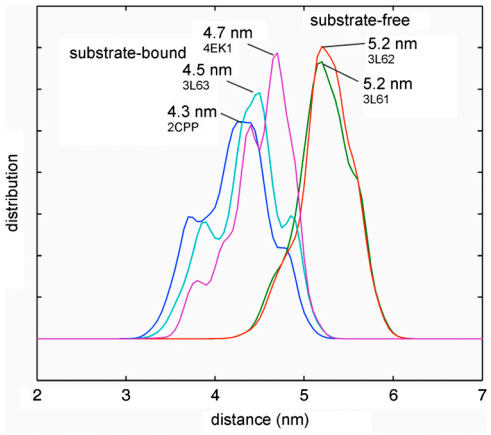

Fig. S3. NO–NO distance distributions for several crystal structures of P450cam in the substrate-bound form (2CPP, 3L63, 4EK1) and the substrate-free form (3L61, 3L62), obtained via rotameric modeling of MTSL at 48C and 190C using MMM2011. 4EK1 is the crystal structure of the spin-labeled protein, all other structures are unlabeled proteins. Rotamer populations modeled at 175 K.

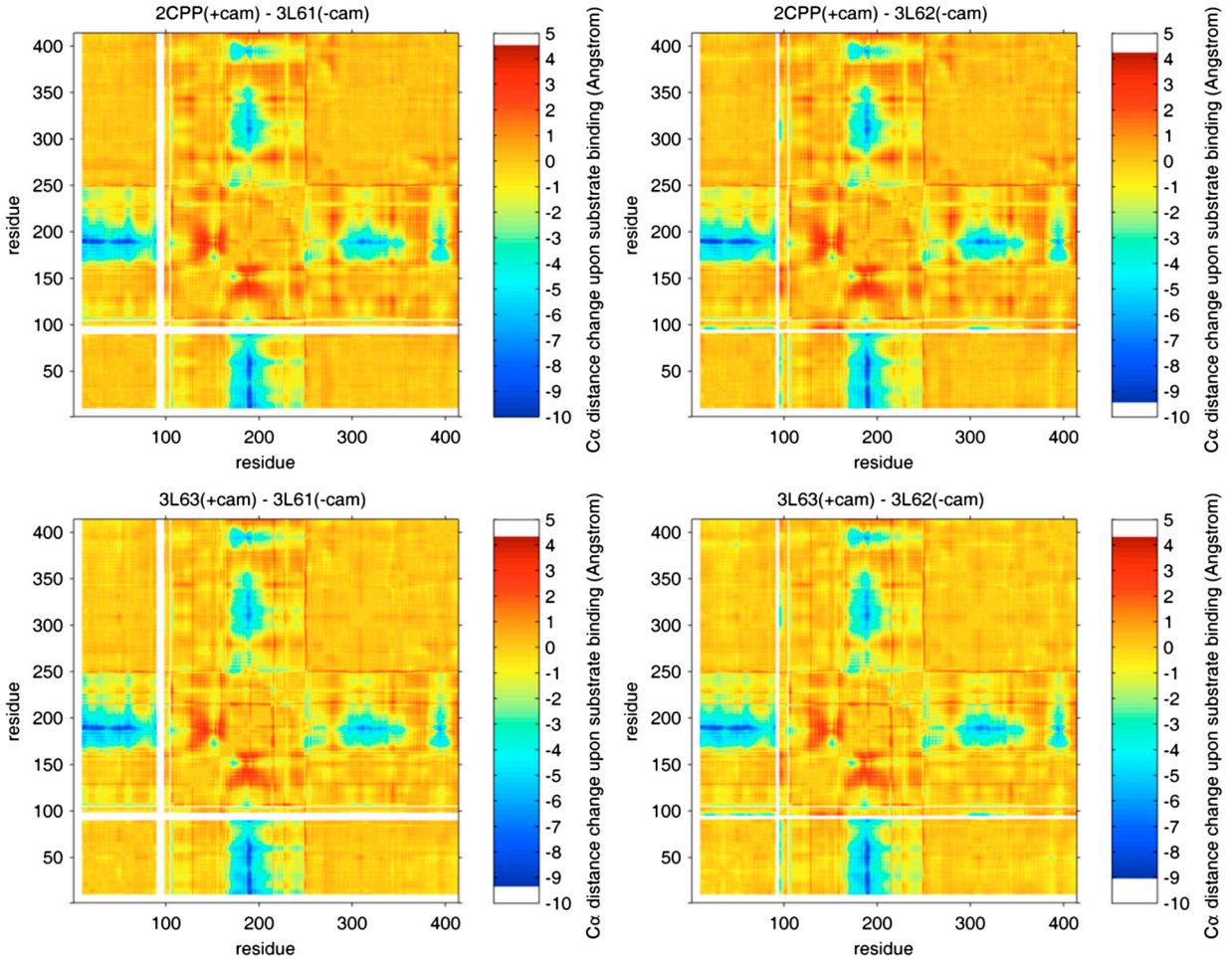

Fig. S4. Predicted Cα–Cα distance changes upon substrate binding for all residues, as obtained from the crystal structures 2CCP (camphor bound, 200 mM $[K^+]$), 3L61 (substrate-free, 200 mM $[K^+]$), 3L62 (substrate-free, low $[K^+]$), and 3L63 (camphor-bound, low $[K^+]$).

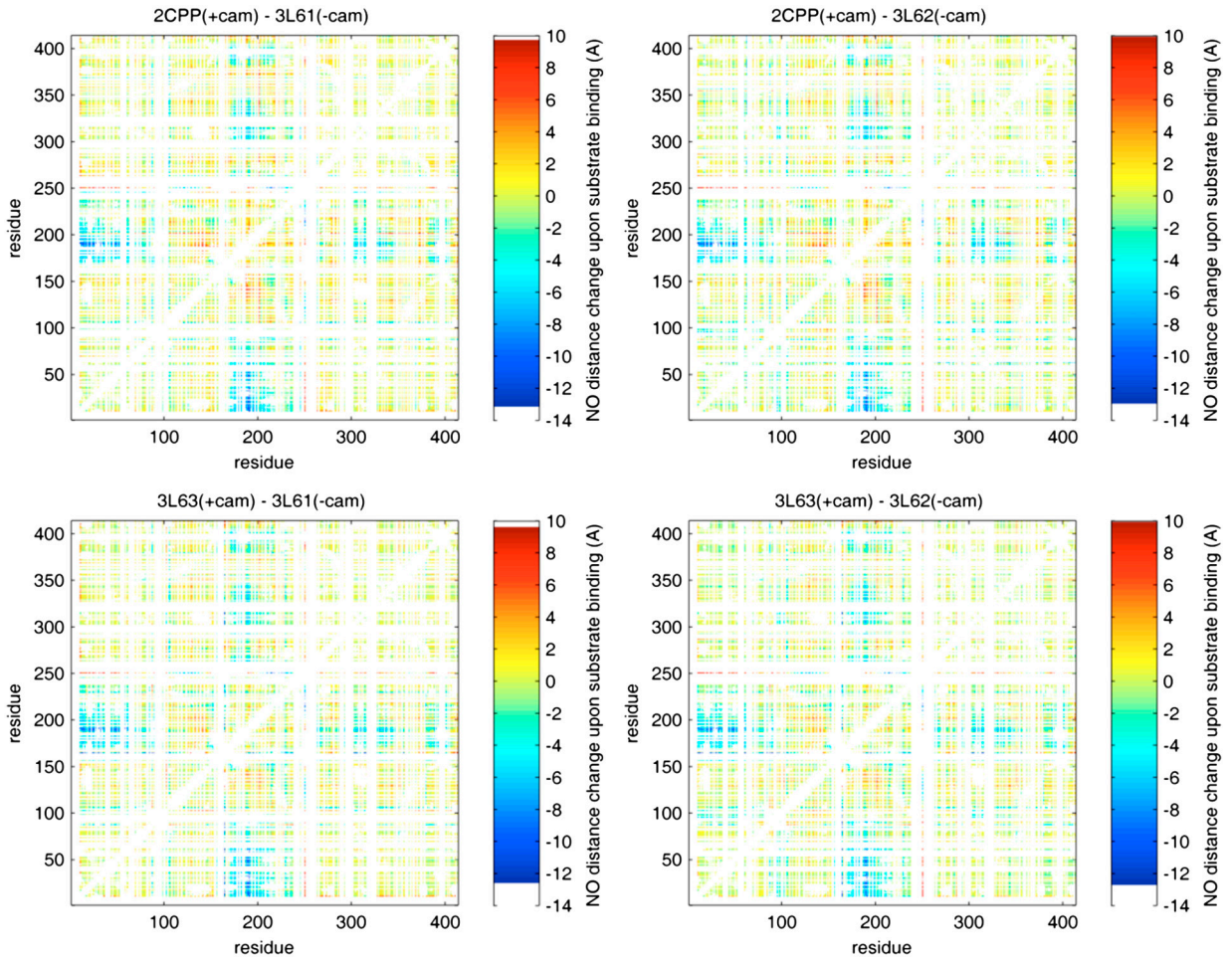

Fig. S5. NO–NO distance changes upon substrate binding predicted by rotamer modeling. Sites with rotamer partition function less than 0.3 (poor labeling) and site pairs with distances below 1.8 nm or above 5.5 nm (outside the optimal range for DEER) are excluded.

Table S1. Data collection, refinement statistics and validation

PDB ID	4EK1
Data collection	
wavelength (Å)	1.12709
unit cell (Å)	56.02, 101.53, 72.98; $\beta = 107.39$
space group	P21
resolution range (Å)	53.46–1.97 (2.07–1.97)*
No. of total reflections	172,235
No. of unique reflections	54,475
Completeness (%)	98.4 (98.6)
R_{merge} (%)	10.1 (41.6)
$<I/\sigma(I)>$	7.7 (2.4)
Refinement statistics	
resolution range (Å)	10–2.0
No. of reflections used	51,287
Free R reflections (%)	5.0
R/R_{free}	0.183/0.233
rmsd bond length (Å)	0.0116
rmsd bond angle (deg)	1.492
Ramachandran analysis (%)	
Residues in	
most favored regions	89.6
additional allowed regions	10.4
generously allowed regions	0.0
disallowed regions	0.0

*Data for the outermost shell are given in the parentheses.

Table S2. Spin label rotamer distribution statistics

	48			190		
	NO rmsd	rotamers	partition function	NO rmsd	rotamers	partition function
2CPP	0.60 nm	160	1.36	0.47 nm	64	0.60
3L63	0.59 nm	162	1.20	0.56 nm	110	1.53
3L62	0.56 nm	155	1.05	0.53 nm	85	1.01
3L61	0.58 nm	154	1.16	0.52 nm	82	1.12
4EK1	0.54 nm	105	1.14	0.53	11	0.11

Table S3. Cα–Cα and NO–NO distances.

	48Cα–190Cα distance (nm) from crystal structures	48NO–190NO average distance (nm) from rotamer models	NO–NO rmsd (nm)
2CPP	3.71	4.28	0.40
3L63	3.76	4.42	0.39
3L62	4.52	5.31	0.31
3L61	4.54	5.29	0.32
4EK1	3.73	4.57	0.35

Table S4. Cα–Cα and NO–NO distance changes upon substrate binding.

	48Cα–190Cα distance change (nm) from crystal structures	48–190 NO distance change (nm) from rotamer models
3L61 → 3L63	−0.78	−1.03
3L61 → 2CPP	−0.83	−1.01
3L61 → 4EK1	−0.81	−0.72
3L62 → 3L63	−0.76	−0.89
3L62 → 2CPP	−0.81	−1.03
3L62 → 4EK1	−0.79	−0.74